



Impact of Se doping on optical and third-order nonlinear optical properties of spray pyrolysis fabricated CdS thin films for optoelectronics

Mohd. Shkir¹ · Mohd. Anis² · S. S. Shaikh³ · Mohamed S. Hamdy⁴ · S. AlFaify¹

Received: 9 October 2019 / Accepted: 2 June 2020 / Published online: 15 June 2020
© Springer-Verlag GmbH Germany, part of Springer Nature 2020

Abstract

Cadmium sulphide is known to have tremendous applications towards optoelectronic and nonlinear devices. Hence, here we have facilely casted the CdS films with diverse Se contents through low-cost spray pyrolysis technique. XRD study defends mono-phase formation of CdS having hexagonal system at all Se doping contents. Scherrer equation was employed to evaluate crystallite size in range of 15–25 nm. Vibrational study reveals the presence of fundamental modes of vibration of hexagonal CdS. EDX and SEM mapping studies approve the existence of Se and its homogeneous distribution all over the film. SEM micrographs shows the nanoscale grains formation on film surface and the size is increasing with Se doping. Optical study revealed that the grown films are of optimal quality with transparency in range of 60–75% with low absorbance and reflectance values. The refractive index values are noted to varied from 1 to 2.7 with wavelength and noticed to be reduced on Se content in UV–Vis region. The reduction in direct and indirect energy gap was found from 2.46 to 2.34 eV and 2.21 to 1.96 eV, correspondingly due to Se. PL emission profile contains an emission band at 528, 529, 529, 530 and 546 nm for 0.0, 0.5, 1.0, 2.5, 5.0 wt% Se:CdS films. Dielectric constant and loss were estimated. The nonlinear refraction (n_2) and absorption coefficient (β) and third-order nonlinear susceptibility (χ^3) values were determined using Z-scan and observed in order of 10^{-8} cm²/W, 10^{-4} cm/W and 10^{-3} esu, correspondingly. The high values of χ^3 propose the films for nonlinear applications.

Electronic supplementary material The online version of this article (<https://doi.org/10.1007/s00340-020-07472-x>) contains supplementary material, which is available to authorized users.

✉ Mohd. Shkir
shkirphysics@gmail.com

✉ S. AlFaify
saalfaiyf@kku.edu.sa

¹ Advanced Functional Materials and Optoelectronic Laboratory (AFMOL), Department of Physics, Faculty of Science, King Khalid University, PO Box 9004, Abha 61413, Saudi Arabia

² Department of Physics and Electronics, Maulana Azad College of Arts, Science and Commerce, Aurangabad, Maharashtra 431001, India

³ Thin Film Physics Laboratory, Department of Physics, Electronics and Photonics, Rajarshi Shahu Mahavidyalaya, Maharashtra, Latur 413512, India

⁴ Chemistry Department, College of Science, King Khalid University, PO Box 9004, Abha 61413, Saudi Arabia

1 Introduction

CdS is a highly applicable semiconductor from II–VI group in several, solar cell, linear, nonlinear, photodetection and other optoelectronic devices. There is a number of literatures on CdS in bulk, nanostructures and nanostructured thin films, etc. that show wide range of applications. The literature reveals that the nanostructured thin films of CdS are highly applicable in most of the devices as mentioned above. Along with pure CdS film fabrication, it is necessary to prepare the films with suitable dopants. Dopants are noticed to play vital character in altering the physical chattels of semi-conducting materials. There are numerous dopants from rare earths, transition metals which are specially applied to semi-conductors to modify their characteristics for future devices.

In recent films CdS have been casted with different dopants like: Sn/Mn:CdS [1], Cu:CdS [2], Fe/Mn:CdS [3], Li-Co:CdS [4], Eu:CdS [5], Ni:CdS [6], B:CdS [7], Ga:CdS [8], Ag:CdS [9], In:CdS [10], Zn/Fe:CdS [11], Sn:CdS [12], F:CdS [13], Al:CdS [14], etc. and displayed the significance of these on physical characteristics of CdS with enhancement for optoelectronics usages. Selenium doping is noticed

to have an immense consequence on structure, vibrational, morphology, optical, nonlinear, dielectric and electrical chattels [15–18].

Pan et al. synthesized the 1D nanostructuring of CdS with Se doping and studied the color-changeable optical transport [19]. Shi et al. prepared the Se:CdS quantum dots with exceptional properties and studied them [20]. Reyes-Banda et al. investigated the role of Se diffusion and CdS layer on CdS/CdTe solar cell performance [21]. Yang et al. organically synthesized the CdS/Se:CdS nanocrystals and studied them [22]. Sankar et al. have grown the CdS crystal with P, Se and Si and studied them [23]. Also Kunioka et al. casted PV cell from CdS on Se layer by vacuum evaporation technique [24]. Akl et al. casted Se:CdS thin films through thermal evaporation [25]. Lacomis et al. thermally evaporated CdS films with Mn, Sb and Se dopant and investigated them [26]. These reports indicate that the properties of CdS have been improved/modified by Se doping, and hence Se is a good dopant.

After reviewing the literature from almost all scientific sources it was noticed that there is no/least report on diverse concentrations of Se in CdS film preparation by spray pyrolysis method and their opto-nonlinear characterizations so far. Hence, we have fabricated the films of Se:CdS (Se = 0.0, 0.5, 1.0, 2.5 and 5.0 wt%) by NSP process on a heated glass substrate at 300 °C. The fabricated films were exposed to X-ray diffraction (XRD) for structural, FT-Raman for vibrational, energy dispersive X-ray spectroscopy (EDX) and scanning electron microscopy (SEM) for elemental, distribution and surface morphology, UV–Vis–NIR spectroscopy for optical, dielectric and nonlinear properties and explained.

2 Experimental procedures

To fabricate the thin films of Se:CdS we have procured CdCl₂·H₂O, thiourea and selenium dioxide from Himedia Pvt. Co. Ltd. Calculated amounts as 0.025 M CdCl₂ and 0.025 M thiourea materials were separately dissolved first in 18 ml of water and ammonia solvent mixture taken in 4:1 ratio. The regular stirring was done throughout the preparation of all solutions at a fixed temperature and rotations were kept around 600 rpm. Both solutions were mixed to achieve CdS and during the mixing different content of Se source, SeO₂ as 0.5–5.0 wt% was dissolved in water and regularly mixed. All solutions' pH was sustained at 11.5. Finally, to fabricate the films all solutions were sprayed on to high-quality and well-cleaned substrates of glass by keeping it at fixed temperature, i.e., ~300 °C. Using this technique the distance between substrate and nozzle, pressure of gas carrier and rate of flow of solution can be varied easily and in the current experiment these were kept as 27 cm, ~1 kg/cm² and 5 ml/m, in that order. After natural cooling of the

system films were taken out and subjected to thickness analyser which shows 450 nm-thick films.

A Shimadzu Lab-X, XRD-6000 (Cu source, $\lambda = 1.54056 \text{ \AA}$) of $\pm 0.001^\circ$ accuracy operating at 40 kV and 30 mA in 10° – 70° angular region on $4^\circ/\text{min}$ scan speed, FT-Raman spectrometer (532 nm excitation source) from Thermo Fisher Scientific, A Japan-made JEOL JSM 6360, EDX and SEM, A Japan-made JASCO V-570, UV–Vis–NIR spectrophotometer and a Thermo Fisher Scientific supplied Lumina fluorescence spectrophotometer were used.

3 Results and discussions

3.1 Structure-vibration studies

The recorded XRD data were transformed to XRD patterns for all films as depicted in Fig. 1a, that clearly indicate the hexagonal polycrystalline films well matched with typical data JCPDS no: 41-1049 and also with former reports on pure and CdS-doped films [27, 28]. Moreover, to have further confirmation about the phase of the prepared films we have determined the lattice constants by POWDERX as listed in Table 1. Data provided in table confirm single hexagonal phase as it well agreed with typical data JCPDS no: 41-1049.

Further, to understand the Se content effect on crystallites size (L), no. of dislocations (δ), strain (ϵ) and unit cell numbers (n) of CdS, we have used the below rules to estimate these [29, 30]: $L = \frac{0.9\lambda}{\beta \cos \theta}$, $\delta = \frac{1}{L^2}$ and $\epsilon = \frac{\beta \cot \theta}{4}$ and $n = \frac{\pi L^3}{6V}$, as presented in Table 1. These data show that the L is lessened with rising of Se content in CdS, which means the films are getting towards amorphous nature. In respect of L values, the values of δ and ϵ are also changing. The values of δ and ϵ are increased with rising the content of Se which indicates more dislocations and strain produced in films by rising the Se content in CdS films. The n values are also reducing with Se content as opposed to δ and ϵ . This means that the films are more deteriorated and hence the film quality decreased with Se content.

To explore impact of Se content on vibrational modes of CdS films the FT-Raman profiles were documented as displayed in Fig. 1b. It is visible for exposed image that the Se contents have strong effect on Raman intensity of CdS peaks. Also, the minute variation in position of peaks was also noticed. The major Raman modes are positioned at 297 and 598 cm⁻¹ in pure and at 301 and 600 cm⁻¹ in 0.5 wt%, at 299 and 601 cm⁻¹ in 1.0 wt%, at 299 and 600 cm⁻¹ in 2.5 wt% and at 302 and 602 cm⁻¹ in 5.0 wt% Se. These respective modes are ascribed to fundamental vibration mode, 1LO and first overtone, 2LO modes and agree well with previous documented literature on CdS [31–33].

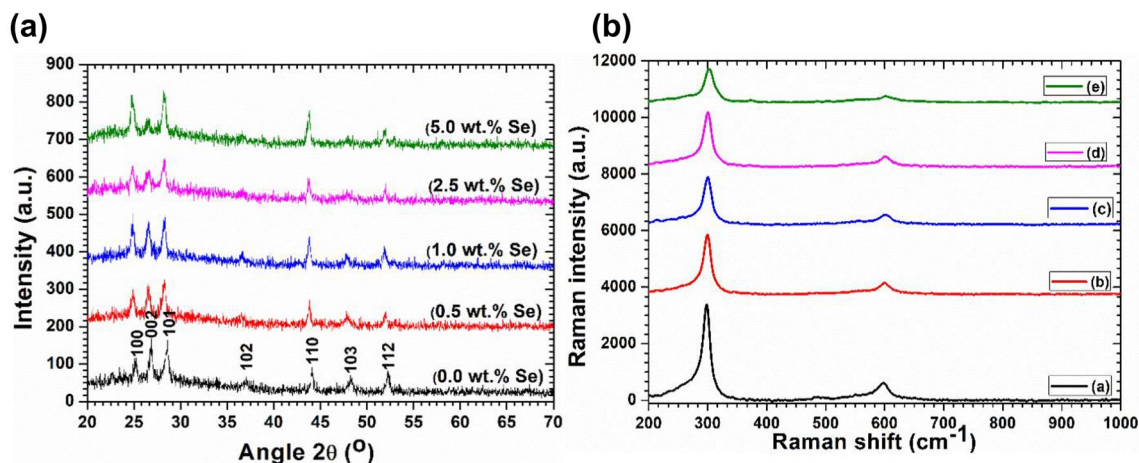


Fig. 1 Profiles for **A** XRD and **B** FT-Raman for spray deposited (a) 0.0 wt%, (b) 0.5 wt%, (c) 1.0 wt%, (d) 2.5 wt% and (e) 5.0 wt% Se: CdS films

Table 1 Assessed values of lattice constants, L , δ and ϵ , and n for Se: CdS films

Samples	$a=b$ (Å)	c (Å)	V (Å) ³	FWHM (β_{002})	L (nm)	δ (nm ⁻²) $\times 10^{-3}$	$\epsilon \times 10^{-3}$	$n \times 10^4$
0.0% Se: CdS	4.13969	6.72784	99.84879	0.4720	17.303	3.340	8.62	2.72
0.5% Se: CdS	4.13715	6.73655	99.85514	0.5281	15.465	4.181	9.79	1.94
1.0% Se: CdS	4.14510	6.73372	100.19747	0.6012	13.584	5.419	11.12	1.31
2.5% Se: CdS	4.13797	6.73010	99.79917	0.7475	10.933	8.378	13.81	0.69
5.0% Se: CdS	4.14865	6.73171	100.33872	0.8364	9.764	10.490	15.55	0.49

3.2 Elemental composition and mapping and surface morphology analyses

For elemental composition and mapping studies the EDX spectra and SEM e-mapped images were captured along with line scan profile and exhibited in Fig. 2a–c. EDX/SEM e-mapping is noticed to be good tool in identification of elements and their homogeneity in final products [34–36]. EDX spectra signify the existence of Cd, S and Se in film and mass % of Cd, S and Se was noticed to be 76.37, 20.56 and 3.07, respectively. Figure 2b indicates the homogeneous distribution of Cd (red), S (green) and Se (blue) molecules all over the film. Line scan profile displayed in Fig. 2c shows the presence of Cd by yellow, S by green and Se by blue colour. This also shows that the concentration of Se is lower while Cd and S are rich which should be the case here. Hence, the existence of Cd, S and Se with high homogeneity was approved from EDX/SEM mapping/line scan measurements [37]. Similar type of observations has been documented previously by several authors on different class of products [38, 39].

SEM are exposed in Fig. 3a–d for 0.5, 1.0, 2.5 and 5.0 wt% Se-doped CdS films. Figure (a) indicates that the 0.5 wt% CdS film contains very low dimension nanograins with some nanocluster formation and the average size of grains and clusters may be in the range between 40 and 200 nm.

Similar type of morphology was seen for pure CdS which we have not included here. When the Se of 1.0 wt% concentration was added the number of grains is noted to be increased and becomes finer and the average size is around 40 nm; however the nanoclusters are still formed of average size 180 nm (see Fig. 3b). Figure 3c, d reveals the surface morphology of 2.5 and 5.0 wt% Se: CdS film, where grains are increased enormously and reduced again with regular distribution thoroughly and compacted on the surface of the films. In all film surface morphology, no crack has been seen which confirms homogeneous thickness of the films throughout and makes them more suitable from device application point of view. Similar kind of surface morphology and cluster formation was reported earlier [36, 38, 40].

3.3 UV–Vis–NIR spectroscopy studies

Figure S1 (a) and (b) (see supplementary data) represents the recorded A , T and R profiles for Se: CdS films up to NIR region. Graph S1 (a) (see supplementary data) indicates that the grown films are having low absorbance and their edge is shifting near higher as well as lower wavelength with Se doping content. This kind of shift in absorption edge signifies the change in energy gap owing to Se content doping in CdS. This may also be due to some other sources like defects and interfaces in films [41]. The optical transparency and

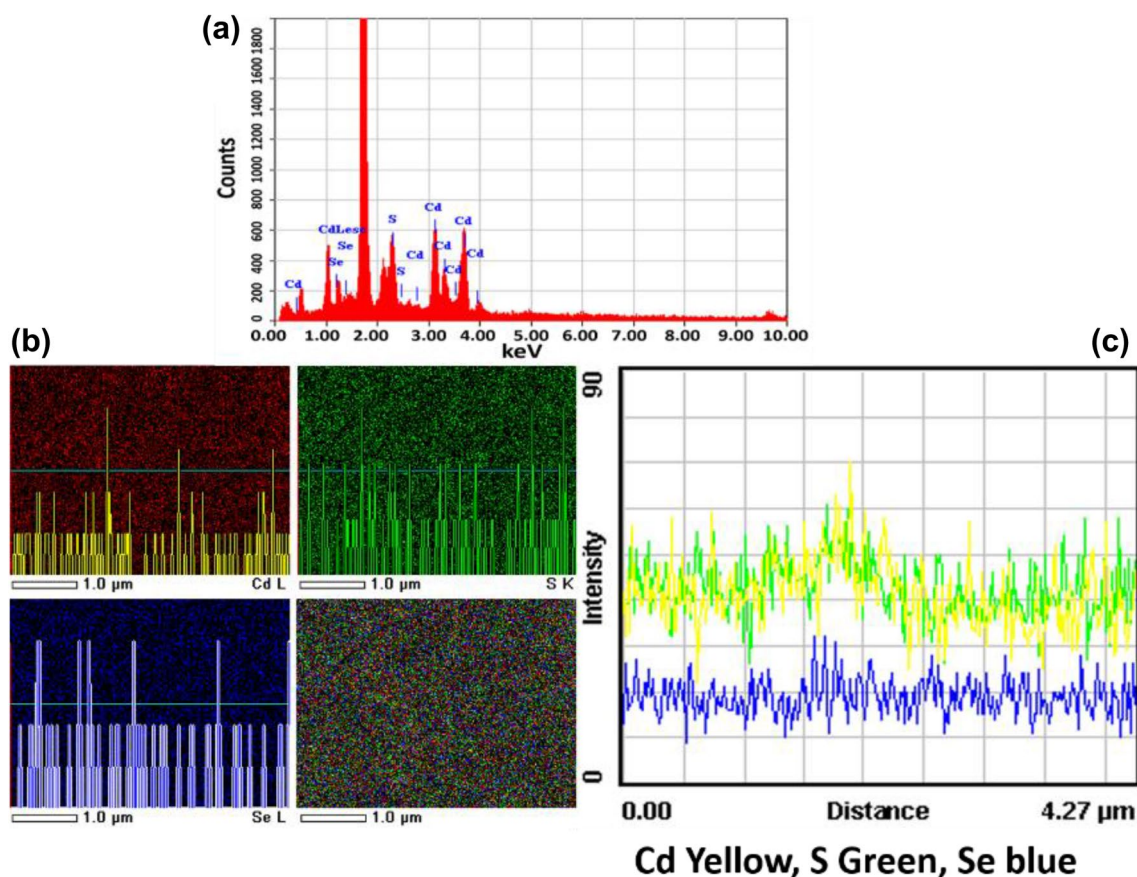


Fig. 2 a EDX spectra, b SEM mapping and c line scan for 5.0 wt% Se:CdS film

reflectance of films are presented in graph S1 (b) (see supplementary data), which shows that the films are transparent enough for optoelectronic device purpose and the transparency is in range from 60 to 78%. The optical transparency of grown films is comparable and even higher than earlier reports on pure and doped CdS films [38, 40, 42–44]. The high transparency and low reflectance propose that the films are quite good from applications point of view. The transparency is noticed to be varied with Se content and minimum was noticed for 0.5 wt% Se:CdS film, though no regular variation was found. Such variation was also reported previously by several authors [45, 46].

Absorption (k) and refractive (n) indices values were estimated through equations: $k = \frac{\alpha\lambda}{4\pi}$ and $n = \frac{(1+R)}{(1-R)} + \sqrt{\frac{4R}{(1-R)^2} - k^2}$ and presented in graphs 4(a) and (b), correspondingly. The graphs (a) provide k values in 0.04–0.25 up to visible region; however, in NIR region its value is noted to be stable and higher number is noted for 0.5 wt% Se:CdS film. The estimated n values are noticed in 1 to 2.7 range for Se:CdS films and indicates the variation owing to Se doping content in CdS. The E_g^d and E_g^i

values were calculated using Tauc's rule [30, 47, 48]: $(\alpha hv)^2 = A(hv - E_g^d)$ and $(\alpha hv)^{0.5} = A(hv - E_g^i)$, correspondingly. Before going to estimate E_g^d and E_g^i , the α values were calculated using the following equation: $\alpha = 2.303 \frac{\text{Absorbance}}{d}$, where d stands for film thickness; then $(\alpha hv)^2$ and $(\alpha hv)^{0.5}$ were attained and designed w.r.t. $E(hv)$ in Fig. 4c, d, correspondingly. By plotting a straight line towards energy axis at $(\alpha hv)^2 = 0$ and $(\alpha hv)^{1/2} = 0$, the values of E_g^d and E_g^i were observed. The E_g^d and E_g^i values are noted in range from 2.46 to 2.33 eV and 2.2 to 1.96 eV. These values are observed to be reduced with Se doping content; however, they agree well with earlier reports [49, 50]. The E_g^d and E_g^i values are lessened from 2.46 eV pure to 2.33 eV and 2.2 to 1.96 eV for 0.5 wt% Se:CdS films. Hence, approved the intense effect of Se content on CdS films optical characteristics. The estimated direct energy gap is noted to be slightly higher compared to bulk CdS [51], which lessens with Se content doping. Decrease/increase in energy gap depends on several factors such as dopant, temperature, thickness, grain/crystallite size, roughness, etc. [35, 36, 52–54].

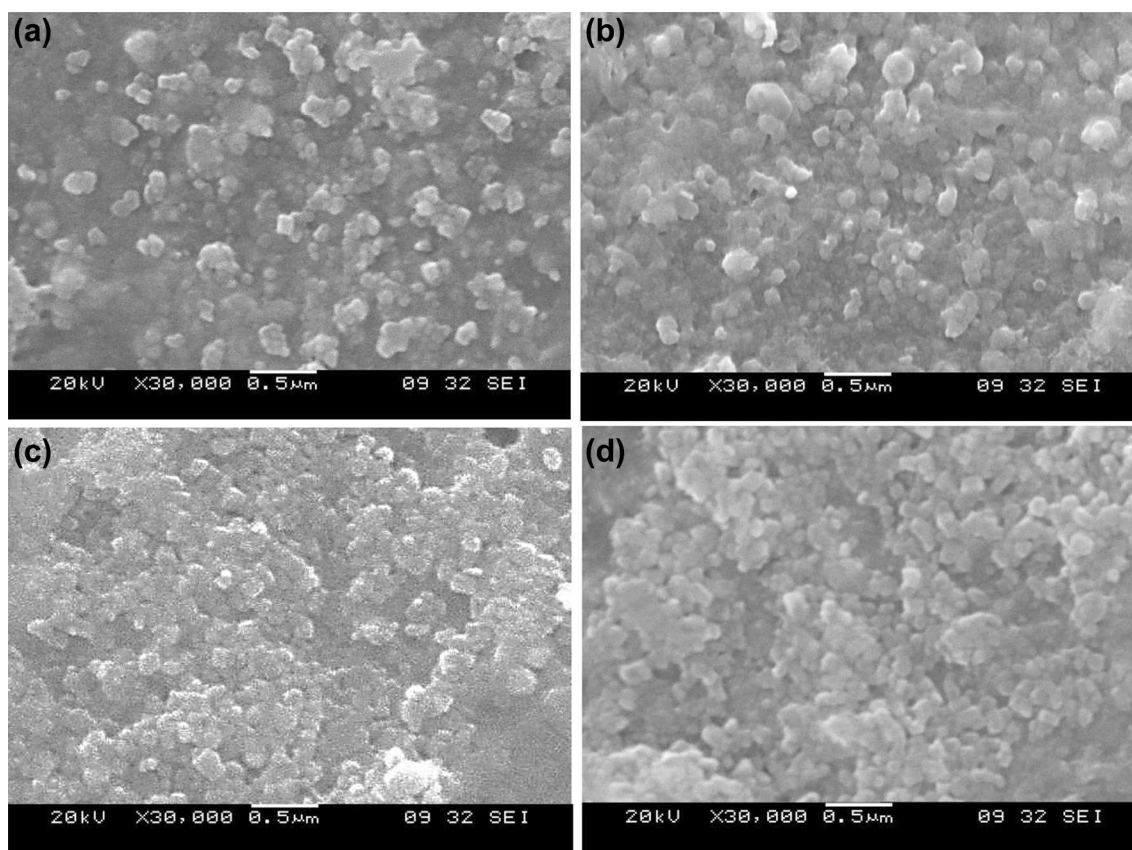


Fig. 3 SEM images for **a** 0.5 wt%, **b** 1.0 wt%, **c** 2.5 wt% and **d** 5.0 wt% Se:CdS films

3.4 PL study

The recorded PL emission profiles for Se:CdS films at $\lambda_{\text{exc}} = 450$ nm are exposed in Fig. 5. Graph clearly displays that there is only one emission peak at around 528 nm in 0.0 wt%, 530 nm in 0.5 wt%, 529 nm in 1.0 wt%, 532 nm in 2.5 wt% and 546 nm in 5.0 wt% Se:CdS films. The observed emission peak may be attributed to intrinsic flaws relating to Cd and S interstitial/vacancies (I_{Cd} , $V_{\text{Cd}}/V_{\text{S}}$), and more explanation can be seen in earlier reports [55, 56]. The emission peaks are noted to shift towards larger wavelength, hence indicating the reduction in energy gap as discussed in above section. Also, the PL emission peak intensity is changing with changing Se doping content. The highest PL emission intensity was observed for 2.5 wt% Se:CdS film; however, the lower intensity was noticed for 5.0 wt% Se:CdS film. Such variation in emission intensity might be owing to defects created from distortedness in the films when doped with Se, which acts as colour centres [57]. The observed emission peak is ascribed to green emission and will be applicable in green LED fabrication. PL emission peaks is owing to band–band emission/emission owing to defects in creation by Se. The PL emission peak observed in current work agrees well with earlier report [27, 58, 59].

3.5 Dielectric and electrical studies

The estimation of both real (ϵ'_r) and imaginary (ϵ''_r) fragments of dielectrics and loss tangent ($\tan \delta$) are quite important to explore the usages of fabricated films as capacitive storing as well as several other applications [60–62]. The intricate form of ϵ'_r and ϵ''_r is expressed as follows: $\epsilon = \epsilon'_r + i\epsilon''_r$. From this equation the ϵ'_r and ϵ''_r can be estimated as [63]: $\epsilon'_r = n^2 - k^2$ and $\epsilon''_r = 2nk$, in that order. The determined values for ϵ'_r , $\tan \delta$, and ϵ''_r are exposed in Fig. S2 (a), (b) and (c) (see supplementary data), in that order. The ϵ'_r , $\tan \delta$, and ϵ''_r values are noticed in range from 1 to 7.5, 0.03 to 0.45, and 0.13 to 0.71, in that order over the whole tested wavelength regions. These ϵ'_r values estimated for currently grown films are comparable to prior documents on CdS [64, 65]. The $\tan \delta$ and ϵ''_r are noticed to be very low, which indicates lesser defects in films. Fig. S2 (d) (see supplementary data) presents the optical conductivity in terms of wavelength calculated from: $\sigma_{\text{oc}} = \frac{anc}{4\pi}$ for all films. The value of σ_{oc} is noticed to be lessened with wavelength [65], but, however, noted to be varied with varying the Se in CdS. The order of σ_{oc} which is around 5 orders explores the applications of fabricated Se:CdS films in optoelectronics and good conductive.

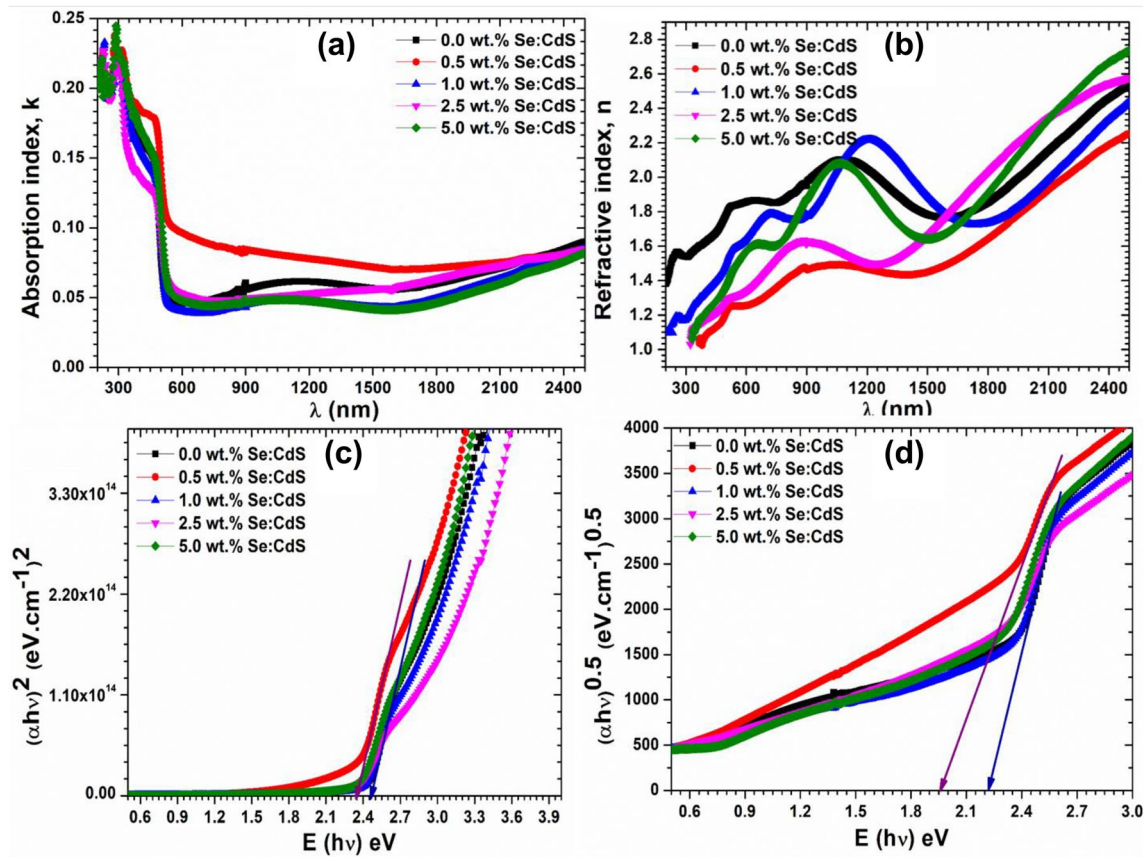


Fig. 4 a k , b n , c $(\alpha h\nu)^2$ vs. $E(h\nu)$ and d $(\alpha h\nu)^{0.5}$ vs. $E(h\nu)$ plots for pure and Se-doped CdS films

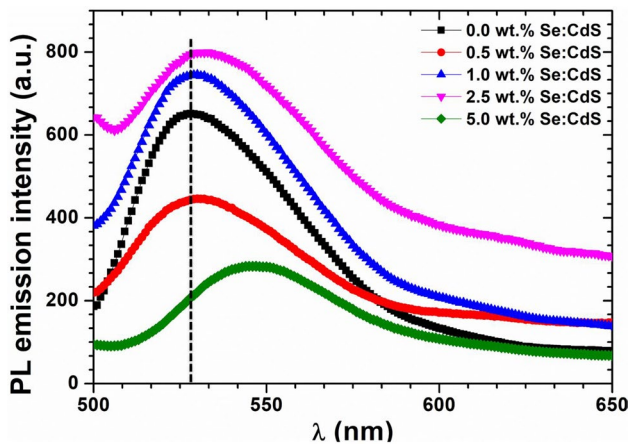


Fig. 5 Recorded PL emission spectra for Se:CdS films at $\lambda_{exc} = 450$ nm

3.6 Nonlinear properties

Z-scan is the decisive tool to investigate the certainty of third-order nonlinear optical (TONLO) properties [66] at given wavelength and explore the respective applications for distinct photonic devices. Herein, the TONLO traits like: n_2 and β were examined by close and open orifice Z-scan analysis. The transmitted optical signal was trailed by photodetector which is mounted far distant along the optical path and the close aperture Z-scan curves of respective thin films are graphed in Fig. 6a–d. It is noticed that the samples offer phase change from peak to valley about the focus that authorises the existence of negative nature of TONLO refraction. This is proof of Se:CdS films inheriting the self-defocusing effect [67]. The attributes of n_2 is governed by intensity of laser beam bombarded with high repetition which dwells the thermal lensing effect causing the phase change in profile of nonlinear refraction along the focus [68].

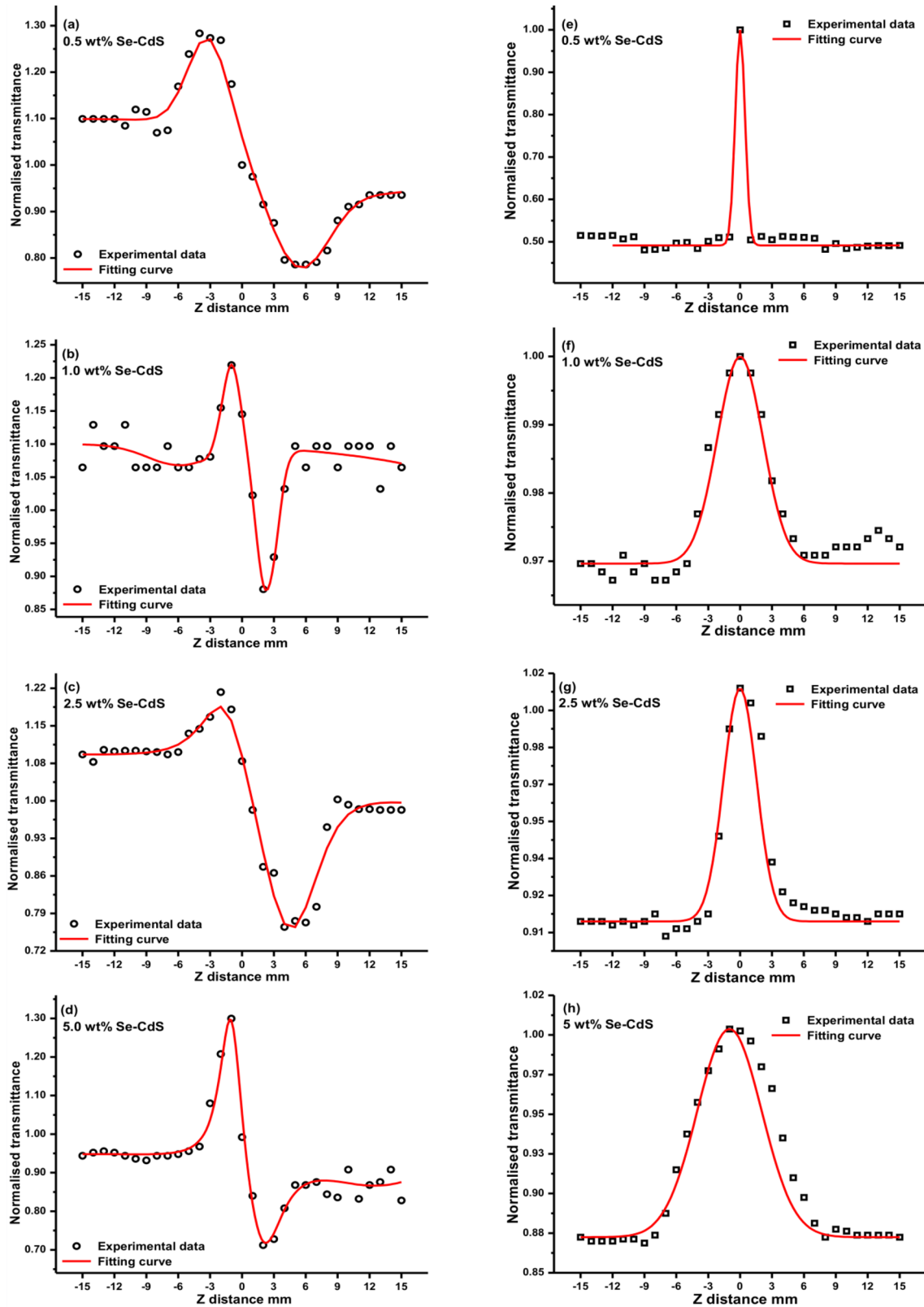


Fig. 6 Z-scan transmittance curve with close (a–d) and open (e–h) aperture

Table 2 TONLO constraints for Se:CdS films

Thin film	n_2 (cm ² /W)	β (cm/W)	χ^3 (esu)
0.5 wt% Se:CdS	3.17×10^{-8}	1.48×10^{-4}	5.04×10^{-3}
1.0 wt% Se:CdS	5.06×10^{-8}	2.64×10^{-4}	6.89×10^{-3}
2.5 wt% Se:CdS	5.91×10^{-8}	3.06×10^{-4}	7.22×10^{-3}
5.0 wt% Se:CdS	6.28×10^{-8}	4.11×10^{-4}	8.95×10^{-3}

The open aperture Z-scan configuration is used to examine the TONLO absorption of thin films and the respective graphs is shown in Fig. 6e–h. The observation reveals that the samples offers the supreme intensity at the focus that approves the presence of saturable absorption (SA) [69]. The physical origin of SA in material is contributed due to the superiority of S_0 linear over S_1 nonlinear absorption coefficient [70, 71]. The ability of materials to polarize is a measure of susceptibility of material [72, 73]; hence the TONLO susceptibility (χ^3) of the thin films has been evaluated. The TONLO parameters of Se:CdS thin films are systematically tabulated in Table 2. The currently evaluated values of TONLO constraints are noted to be comparable with earlier reports on In:CdS films [37]. However, estimated values are very high compared to several previously reported values for metals/particles and films [74–77]. The previously reported values of TONLO constraints on diverse class of materials are tabulated in Table 3 for better comparison with current ones.

4 Conclusion

CdS films using 0.5, 1.0, 2.5 and 5.0 wt% Se doping were fabricated facilely through cost-effective spray pyrolysis method. The XRD study defends hexagonal single-phase formation of Se:CdS films. The crystallite size values were estimated in range of 15–25 nm. The fundamental modes of vibration of hexagonal CdS were exposed by vibrational study. The presence of Se and its homogeneous spreading all over the film was shown by EDX and SEM mapping studies. The nanostructured films fabrication was approved from SEM analysis and shows that the size of grains increased with Se doping owing to formation of nanoclusters. The grown films are of optimal quality with transparency in range of 60–75%. The linear refractive index values are found to be varied between 1 and 2.7. Direct and indirect E_g values are found to be lessened due to Se doping from 2.46 to 2.34 eV and 2.21 to 1.96 eV, harmoniously. The emission spectra possess emission peaks at 528, 529, 529, 530 and 546 nm for 0.0, 0.5, 1.0, 2.5, 5.0 wt% Se:CdS films. Dielectric constant was noted in range from 1 to 7.5. The open and close aperture Z-scan studies were performed to find n_2 , β and χ^3 and found to be enhanced from 3.17 to 6.28 ($\times 10^{-8}$) cm²/W, 1.48 to 4.11 ($\times 10^{-4}$) cm/W and 5.04 – 8.95 ($\times 10^{-3}$) esu, correspondingly. Such large third-order nonlinear susceptibility values suggest the nonlinear applications of fabricated films.

Table 3 Comparative NLO parameters reported for various films

Authors	Materials	$\chi^{(1)}$	$\chi^{(3)}$ (esu)	n^2 (esu)
Khan et al. [78]	F:CdS	0.1–0.8	0.02×10^{-11} – 5.5×10^{-11}	1.8×10^{-12} – 6.1×10^{-10}
Shkir et al. [38]	Te:CdS	0.05–0.70	4×10^{-13} – 3.5×10^{-11}	2.4×10^{-14} – 5.5×10^{-10}
Shkir et al. [79]	Mg:ZnO	0.14–0.6	1.0×10^{-13} – 1.0×10^{-11}	2.0×10^{-13} – 1.5×10^{-10}
Khan et al. [80]	Ag:CdS	0.10–7.0	2.92×10^{-10} – 1×10^{-7}	1×10^{-9} – 2×10^{-7}
Radaf et al. [81]	F:CdS	–	1.74×10^{-12} – 16.6×10^{-12}	2.9×10^{-11} – 21.9×10^{-11}
Shkir et al. [37]	In:CdS	–	4.67×10^{-1} – 7.01×10^{-1}	2.14×10^{-7} – 4.99×10^{-7}
Arif et al. [82]	N:ZnO	0.3–9	1.0×10^{-11} – 1.0×10^{-8}	1.4×10^{-12} – 2.5×10^{-8}
Abrinaei et al. [83]	Al:ZnO	–	1.1×10^{-5} – 10.9×10^{-4}	-8.05×10^{-9} – 11.05×10^{-9}
Current work	Se:CdS	–	5.04×10^{-3} – 8.95×10^{-3}	3.17×10^{-8} – 6.28×10^{-8}

Acknowledgements The authors would like to express their gratitude to Deanship of Scientific Research at King Khalid University for funding this work through Research Groups Program under Grant no. R.G.P2/95/41.

Compliance with ethical standards

Conflict of interest Authors have no conflict of interest to show.

References

- K. Karthik, S. Pushpa, M. Madhukara Naik, M. Vinuth, *Mater. Res. Innov.* **24**(2), 82–86 (2020)
- A.A. Aboud, A. Mukherjee, N. Revaprasadu, A.N. Mohamed, *J. Mater. Res. Technol.* **8**(2), 2021–2030 (2019)
- R. Murugesan, S. Sivakumar, K. Karthik, P. Anandan, M. Haris, *Appl. Phys. A* **125**, 281 (2019)
- P. Samiyammal, K. Parasuraman, A.R. Balu, *Superlattices Microstruct.* **129**, 28–39 (2019)
- S. Yilmaz, I. Polat, M. Tomakin, E. Bacaksız, *Appl. Phys. A* **125**, 67 (2019)
- I. Yahia, I. El Radaf, A. Salem, G. Sakr, *J. Alloys Compd.* **776**, 1056–1062 (2019)
- J. Lee, *Thin Solid Films* **451**, 170–174 (2004)
- H. Khallaf, G. Chai, O. Lupan, L. Chow, S. Park, A. Schulte, *Appl. Surf. Sci.* **255**, 4129–4134 (2009)
- M. Ristova, M. Ristov, *Sol. Energy Mater. Sol. Cells* **53**, 95–102 (1998)
- G. Perna, V. Capozzi, M. Ambrico, V. Augelli, T. Ligonzo, A. Minafra, L. Schiavulli, M. Pallara, *Thin Solid Films* **453–454**, 187–194 (2004)
- K. Liu, J. Zhang, X. Wu, B. Li, B. Li, Y. Lu, X. Fan, D. Shen, *Phys. B Condens. Matter* **389**, 248–251 (2007)
- A. Jafari, A. Zakaria, Z. Rizwan, M.S.M. Ghazali, *Int. J. Mol. Sci.* **12**, 6320–6328 (2011)
- S. Yilmaz, *Appl. Surf. Sci.* **357**, 873–879 (2015)
- A. Fernández-Pérez, C. Navarrete, P. Valenzuela, W. Gacitúa, E. Mosquera, H. Fernández, *Thin Solid Films* **623**, 127–134 (2017)
- T. Berus, J. Goc, M. Nowak, M. Oszałdowski, M. Zimpel, *Thin Solid Films* **111**, 351–366 (1984)
- J. Goral, S.R. Kurtz, J. Olson, A. Kibbler, *J. Electron. Mater.* **19**, 95–99 (1990)
- Y. Gong, Z. Liu, A.R. Lupini, G. Shi, J. Lin, S. Najmaei, Z. Lin, A.L. Elias, A. Berkdemir, G. You, *Nano Lett.* **14**, 442–449 (2013)
- J. Henry, K. Mohanraj, S. Kannan, S. Barathan, G. Sivakumar, *Eur. Phys. J. Appl. Phys.* **61**, 10301 (2013)
- A. Pan, X. Wang, P. He, Q. Zhang, Q. Wan, M. Zacharias, X. Zhu, B. Zou, *Nano Lett.* **7**, 2970–2975 (2007)
- J.-W. Shi, D. Sun, Y. Zou, D. Ma, C. He, X. Ji, C. Niu, *Chem. Eng. J.* **364**, 11–19 (2019)
- M.G. Reyes-Banda, E. Regalado-Perez, M.I. Pintor-Monroy, C.A. Hernández-Gutiérrez, M.A. Quevedo-López, X. Mathew, *Superlattices Microstruct.* **133**, 106219 (2019)
- D. Yang, S. Xu, Q. Chen, W. Wang, *Colloids Surf. A* **299**, 153–159 (2007)
- N. Sankar, C. Sanjeeviraja, K. Ramachandran, *J. Cryst. Growth* **243**, 117–123 (2002)
- A. Kunioka, Y. Sakai, *Solid State Electron.* **8**, 961–965 (1965)
- A.A. Akl, A.S. Hassanien, *Superlattices Microstruct.* **85**, 67–81 (2015)
- F. Iacomi, M. Purica, E. Budianu, D. Macovei, *Synthesis of the transparent and conductive CdS thin films for optoelectronic devices applications. In CAS 2005 Proceedings. 2005 International Semiconductor Conference, 2005.2005*, vol. 161, pp. 161–164
- A. Khan, M. Shkir, M.A. Manthrammel, V. Ganesh, I.S. Yahia, M. Ahmed, A.M. El-Toni, A. Aldalbahi, H. Ghaithan, S. AlFaify, *Ceram. Int.* **45**, 10133–10141 (2019)
- R. Bairy, A. Jayarama, G.K. Shivakumar, S.D. Kulkarni, S.R. Maidur, P.S. Patil, *Phys. B Condens. Matter* **555**, 145–151 (2019)
- M. Shkir, S. AlFaify, *Sci. Rep.* **7**, 16091 (2017)
- M. Shkir, M.T. Khan, S. AlFaify, *Appl. Nanosci.* **9**(7), 1417–1426 (2019)
- H.L. Lee, I.A. Mohammed, M. Belmahi, M.B. Assouar, H. Rinnert, M. Alnot, *Materials* **3**, 2069–2086 (2010)
- C. Hu, X. Zeng, J. Cui, H. Chen, J. Lu, *J. Phys. Chem. C* **117**, 20998–21005 (2013)
- H.I. Salim, O.I. Olusola, A.A. Ojo, K.A. Urasov, M.B. Der-gacheva, I.M. Dharmadasa, *J. Mater. Sci.: Mater. Electron.* **27**, 6786–6799 (2016)
- A. Petruhins, J. Lu, L. Hultman, J. Rosen, *Mater. Res. Lett.* **7**, 446–452 (2019)
- M. Shkir, I.M. Ashraf, S. AlFaify, A.M. El-Toni, M. Ahmed, A. Khan, *Ceram. Int.* **46**(4), 4652–4663 (2020)
- M. Shkir, Z.R. Khan, M. Anis, S.S. Shaikh, S. AlFaify, *Chin. J. Phys.* **63**, 51–62 (2020)
- M. Shkir, M. Anis, S.S. Shaikh, S. AlFaify, *Superlattices Microstruct.* **133**, 106202 (2019)
- M. Shkir, S. Shaikh, S. AlFaify, *J. Mater. Sci. Mater. Electron.* **30**, 17469–17480 (2019)
- H. Ding, Y. Li, J. Lu, K. Luo, K. Chen, M. Li, P.O. Å. Persson, L. Hultman, P. Eklund, S. Du, Z. Huang, Z. Chai, H. Wang, P. Huang, Q. Huang, *Mater. Res. Lett.* **7**, 510–516 (2019)
- V. Soleimanian, M. Saeedi, A. Mokhtari, *Mater. Sci. Semicond. Process.* **30**, 118–127 (2015)
- A. Kaushal, D. Kaur, *Sol. Energy Mater. Sol. Cells* **93**, 193–198 (2009)
- S.D. Gunjal, Y.B. Kholam, S.A. Arote, S.R. Jadhkar, P.N. Shelke, K.C. Mohite, *Macromol. Symposia* **347**, 9–15 (2015)
- A.H. Rubel, J. Podder, *J. Bangl. Acad. Sci.* **39**, 25–30 (2015)
- A.A. Aboud, A. Mukherjee, N. Revaprasadu, A.N. Mohamed, *J. Mater. Res. Technol.* **8**, 2021–2030 (2019)
- M. Shkir, A. Khan, A.M. El-Toni, A. Aldalbahi, I.S. Yahia, S. AlFaify, *J. Phys. Chem. Solids* **130**, 189–196 (2019)
- M.T. Khan, M. Shkir, A. Almohammed, S. AlFaify, *Solid State Sci.* **90**, 95–101 (2019)
- S. AlFaify, M. Shkir, *Opt. Mater.* **88**, 417–423 (2019)
- S. AlFaify, M. Shkir, *J. Nanoelectron. Optoelectron.* **14**, 255–260 (2019)
- A. Cortes, H. Gómez, R.E. Marotti, G. Riveros, E.A. Dalchiele, *Sol. Energy Mater. Sol. Cells* **82**, 21–34 (2004)
- O. Zelaya-Angel, L. Hernandez, O. de Melo, J.J. Alvarado-Gil, R. Lozada-Morales, C. Falcony, H. Vargas, R. Ramirez-Bon, *Vacuum* **46**, 1083–1085 (1995)
- C. Grovenor, *Microelectronic materials* (Adam Hilger, Bristol, 1989)
- M. Shkir, S. AlFaify, *J. Mater. Res.* **34**, 2765–2774 (2019)
- Y. Akaltun, M.A. Yıldırım, A. Ateş, M. Yıldırım, *Opt. Commun.* **284**, 2307–2311 (2011)
- S.-Y. Kuo, W.-C. Chen, F.-I. Lai, C.-P. Cheng, H.-C. Kuo, S.-C. Wang, W.-F. Hsieh, *J. Cryst. Growth* **287**, 78–84 (2006)
- S. Yilmaz, İ. Polat, M. Tomakin, T. Küçükömeroğlu, S.B. Törel, E. Bacaksız, *Appl. Phys. A* **124**, 502–508 (2018)
- S. Yilmaz, İ. Polat, M. Tomakin, S. Törel, T. Küçükömeroğlu, E. Bacaksız, *J. Mater. Sci. Mater. Electron.* **29**, 14774–14782 (2018)
- M. Shkir, *J. Mater. Res.* **31**, 1046–1055 (2016)
- M. Shkir, I. Ashraf, K.V. Chandekar, I. Yahia, A. Khan, H. Algarni, S. AlFaify, *Sens. Actuators A* **301**, 111749 (2020)

59. M. Shkir, M. Anis, S. Shafik, M.A. Manthrammel, M. Sayeed, M.S. Hamdy, S. AlFaify, *Physica E Low Dimens. Syst. Nanostruct.* **118**, 113955 (2020)
60. K. Usha, R. Sivakumar, C. Sanjeeviraja, *J. Appl. Phys.* **114**, 123501 (2013)
61. D. Panda, T.-Y. Tseng, *Thin Solid Films* **531**, 1–20 (2013)
62. M.V. Fischetti, W.G. Vandenberghe, *Dielectric Properties of Semiconductors, Advanced Physics of Electron Transport in Semiconductors and Nanostructures* (Springer, Berlin, 2016), pp. 223–251
63. M.-S. Kim, K.-G. Yim, J.-S. Son, J.-Y. Leem, *Bull. Korean Chem. Soc.* **33**, 1235–1241 (2012)
64. M. Shkir, I.M. Ashraf, K.V. Chandekar, I.S. Yahia, A. Khan, H. Algarni, S. AlFaify, *Sens. Actuators A Phys.* **301**, 111749 (2020)
65. P.P. Sahay, R.K. Nath, S. Tewari, *Cryst. Res. Technol.* **42**, 275–280 (2007)
66. M. Sheik-Bahae, A.A. Said, T.-H. Wei, D.J. Hagan, E.W. Van Stryland, *Quantum Electron. IEEE J.* **26**, 760–769 (1990)
67. M.A. Manthrammel, M. Shkir, M. Anis, S.S. Shaikh, H.E. Ali, S. AlFaify, *Opt. Mater.* **100**, 109696 (2020)
68. Z.S. Fadhul, E.A. Ali, S.R. Maidur, P.S. Patil, M. Shkir, F.Z. Henari, *J. Nonlinear Opt. Phys. Mater.* **27**, 1850012 (2018)
69. M. Shkir, P. Patil, M. Arora, S. AlFaify, H. Algarni, *Spectrochim. Acta Part A Mol. Biomol. Spectrosc.* **173**, 445–456 (2017)
70. M. Anis, M. Shkir, M.I. Baig, S.P. Ramteke, G.G. Muley, S. AlFaify, H.A. Ghramh, *J. Mol. Struct.* **1170**, 151–159 (2018)
71. M. Anis, G. Muley, M. Shkir, S. AlFaify, H. Ghramh, *Mater. Sci. Pol.* **36**, 662–667 (2018)
72. R.B. Kulkarni, M. Anis, S. Hussaini, M.D. Shirsat, *Mater. Res. Express* **5**, 036204 (2018)
73. S.R. Maidur, P.S. Patil, S.V. Rao, M. Shkir, S. Dharmaprakash, *Opt. Laser Technol.* **97**, 219–228 (2017)
74. R. Ganeev, A. Rysnyansky, S.R. Kamalov, M. Kodirov, T. Usmanov, *J. Phys. D Appl. Phys.* **34**, 1602 (2001)
75. R.A. Ganeev, M. Baba, M. Morita, D. Rau, H. Fujii, A.I. Rysnyansky, N. Ishizawa, M. Suzuki, H. Kuroda, *J. Opt. A Pure Appl. Opt.* **6**, 447–453 (2004)
76. N. Venkatram, D.N. Rao, M.A. Akundi, *Opt. Express* **13**, 867–872 (2005)
77. W. Cun-Xiu, F. Shi-Shu, G. Yu-Zong, *Chin. Phys. Lett.* **26**, 097804 (2009)
78. Z.R. Khan, M. Shkir, V. Ganesh, S. AlFaify, I.S. Yahia, H.Y. Zahran, *J. Electron. Mater.* **47**, 5386–5395 (2018)
79. M. Shkir, M. Arif, V. Ganesh, M.A. Manthrammel, A. Singh, I.S. Yahia, S.R. Maidur, P.S. Patil, S. AlFaify, *J. Mol. Struct.* **1173**, 375–384 (2018)
80. Z.R. Khan, M. Shkir, A.S. Alshammari, V. Ganesh, S. AlFaify, M. Gandouzi, *J. Electron. Mater.* **48**, 1122–1132 (2019)
81. I. El Radaf, T.A. Hameed, I. Yahia, *Mater. Res. Express* **5**, 066416 (2018)
82. M. Arif, M. Shkir, S. AlFaify, A. Sanger, P.M. Vilarinho, A. Singh, *Opt. Laser Technol.* **112**, 539–547 (2019)
83. F. Abrinaei, M. Shirazi, *J. Mater. Sci. Mater. Electron.* **28**, 17541–17550 (2017)

Publisher's Note Springer Nature remains neutral with regard to jurisdictional claims in published maps and institutional affiliations.